

Radiation-induced magnetoresistance oscillations with massive Dirac fermions.

Jesús Iñarraea^{1,2} and Gloria Platero^{2,3}

¹*Escuela Politécnica Superior, Universidad Carlos III, Leganes, Madrid, 28911, Spain*

²*Instituto de Ciencia de Materiales, CSIC, Cantoblanco, Madrid, 28049, Spain.*

³*Unidad Asociada al Instituto de Ciencia de Materiales, CSIC, Cantoblanco, Madrid, 28049, Spain.*

We report on a theoretical study on the rise of radiation-induced magnetoresistance oscillations in two-dimensional systems of massive Dirac fermions. We study the bilayer system of monolayer graphene and hexagonal boron nitride (h-BN/graphene) and the trilayer system of hexagonal boron nitride encapsulated graphene (h-BN/graphene/h-BN). We extend the radiation-driven electron orbit model that was previously devised to study the same oscillations in two-dimensional systems of Schrödinger electrons (GaAs/AlGaAs heterostructure) to the case of massive Dirac fermions. In the simulations we obtain clear oscillations for radiation frequencies in the terahertz and far-infrared bands. We investigate also the power and temperatures dependence. For the former we obtain similar results as for Schrödinger electrons and predict the rise of zero resistance states. For the latter we obtain a similar qualitative dependence but quantitatively different when increasing temperature. While in GaAs the oscillations are wiped out in a few degrees, interestingly enough, for massive Dirac fermions, we obtain observable oscillations for temperatures above 100 K and even at room temperature for the higher frequencies used in the simulations.

PACS numbers:

I. INTRODUCTION

Radiation-induced magnetoresistance (R_{xx}) oscillations (MIRO)^{1,2} were unexpectedly discovered two decades ago when a high mobility two dimensional electron gas (GaAs/AlGaAs heterostructure) under a vertical magnetic field (B) was irradiated with microwaves (MW). Previously, an influential and pioneering theoretical work on these systems under similar conditions, (in a constant B under radiation), had been already carried out by Ryzhii⁶ in the 70's. Both B and the temperature (T) used in the experiment were very low, $T \sim 1K$ and $B < 1T$. Along with this effect it was discovered also radiation-induced zero resistance states^{1,2} (ZRS) when the radiation power (P) was sufficiently increased. These effects, which suggested a novel way of radiation-matter interaction³⁻⁵, received a lot of attention by the condensed matter community. Thus, many experimental⁷⁻²³ and theoretical²⁴⁻⁴⁰ works have been carried out since their discovery. In this way, they have been obtained in a wide range of two-dimensional (2D) platforms: GaAs/AlGaAs^{1,2} and Ge/SiGe heterostructures⁴¹, 2D electrons on liquid Helium⁴² and in the system MgZnO/ZnO⁴³. The MIRO obtained in all of them share the same features in terms of frequency, power and temperature dependence. Besides, the oscillations minima are always 1/4 cycle shifted irrespective of the platform and carrier. Thus we can conclude that MIRO represents a universal effect and a novel demonstration of radiation-matter interaction in 2D systems.

A natural extension of MIRO would be their study on graphene⁴⁴ systems that we can consider paradigmatic in terms of 2D systems. In graphene the carriers are massless Dirac fermions and in principle it is not clear that they will couple with radiation to give MIRO in the same

way as the Schrödinger electrons do. Even in the case that MIRO could be obtained, it is not clear either if they would keep all of the universal features that define MIRO or just a part of them. Nevertheless, it has been recently reported a remarkable theoretical work that predicts the appearance of radiation-induced resistance oscillations in monolayer and bilayer graphene⁴⁵. In the same way an experimental work⁴⁶ has been published indicating that MIRO can be obtained in h-BN encapsulated graphene keeping most of MIRO characteristics.

In this article, we focus on the presence of MIRO in gapped monolayer graphene systems. More specifically, we study the bilayer system of monolayer graphene on top of hexagonal boron nitride (h-BN) and the trilayer system of h-BN encapsulated monolayer graphene. In both systems the carriers are *massive* Dirac fermions⁴⁷⁻⁵². The latter is more in deep analyzed because it presents one of the highest mobilities ($\mu \sim 3 \times 10^5 \text{ cm}^2/Vs$) among the graphene systems and a high mobility is essential to clearly observe MIRO. In our simulations we apply the theoretical model of *radiation-driven electron orbits*^{24,25} successfully applied to Schrödinger electrons systems to address MIRO and ZRS. For massive Dirac fermions we recover magnetoresistance oscillations with an important difference in terms of radiation frequency: according to our model, these graphene systems are sensitive to terahertz (THz) and far-infrared frequencies instead of MW, giving rise to terahertz-induced resistance oscillations (TIRO). Nevertheless, TIRO keep similar P and T dependence as MIRO. In the case of P we obtain that as P rises, the oscillations amplitude rises as well following a sublinear law close to a square root dependence. We also predict the rise of ZRS for massive Dirac fermions when P is high enough, as in MIRO. In the case of T , we recover that oscillations decrease in amplitude for increasing T . However, TIRO survive at much higher

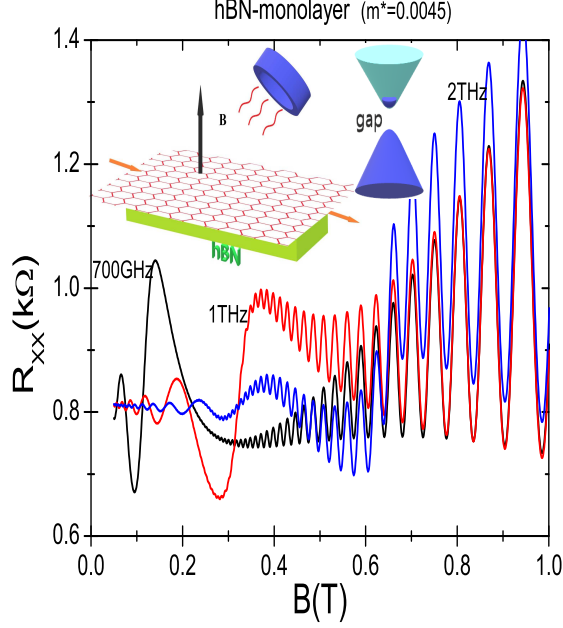


FIG. 1: Calculated magnetoresistance R_{xx} under radiation vs magnetic field for a bilayer of h-BN and monolayer graphene. The three curves correspond to frequencies of 700GHz, 1THz and 2THz. The oscillations amplitude gets smaller as frequency increases (for $B < 0.7$ T). The inset displays a schematic diagram of the experimental setup basic features and the band diagram of gapped monolayer graphene. $T = 1$ K.

T than the usual MIRO that are completely wiped out when increasing T only a few degrees. For TIRO we observe clear oscillations up to 100 K for all simulations and even at room temperature (300 K) for the highest frequencies used (2.0 THz).

II. THEORETICAL MODEL

Monolayer graphene is a 2D network of carbon atoms organized in an hexagonal lattice that can be described as a triangular Bravais structure with two atoms per unit cell denoted by A and B. In the reciprocal lattice we obtain an hexagonal shaped Brillouin zone where two out of the six corners are inequivalent. They are denoted as K and K' . When monolayer graphene is placed on top of a definite material (substrate), yielding a Van der Waals heterostructure, the interaction between graphene and the substrate gives rise to different potentials between the locations A and B, breaking the carbon sublattice symmetry^{53,54}. As a result of this potential asymmetry a band gap opens at the Dirac point producing gapped monolayer graphene (see insets of Figs. 1 and 2). Thus, monolayer graphene turns from semimetal into a semiconductor, and remarkably enough, the Dirac fermions

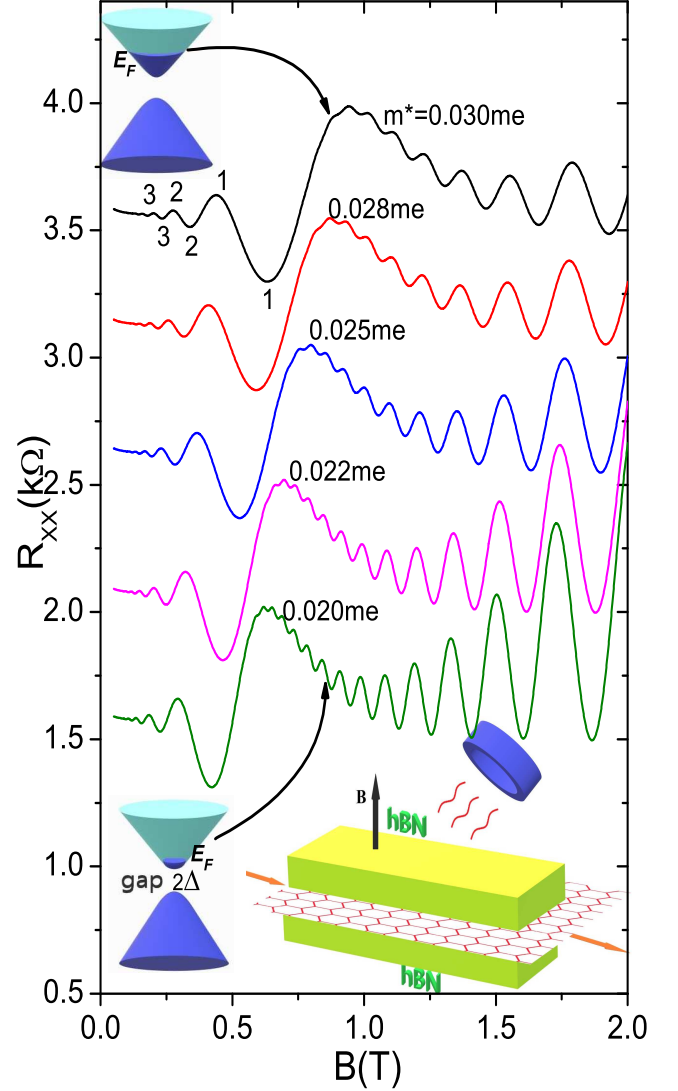


FIG. 2: Calculated magnetoresistance R_{xx} under radiation vs magnetic field for h-BN encapsulated monolayer graphene (hBN-monolayer graphene-hBN). The radiation frequency is 700GHz. Five curves are exhibited corresponding to five different effective masses or bandgaps. Every effective mass corresponds to a different bias between the hBN layers (top and bottom). The inset shows a schematic diagram of the h-BN sandwiched monolayer graphene under a constant magnetic field and radiation. We present also two schematic band diagrams of gapped graphene. The lower one corresponds to the lowest external bias and the lowest Fermi energy (green curve). The upper one corresponds to the highest bias and the highest Fermi energy (black curve). $T = 1$ K.

become massive.

The Hamiltonian for the gapped monolayer graphene with a perpendicular magnetic field $\vec{B} = (0, 0, B)$, for

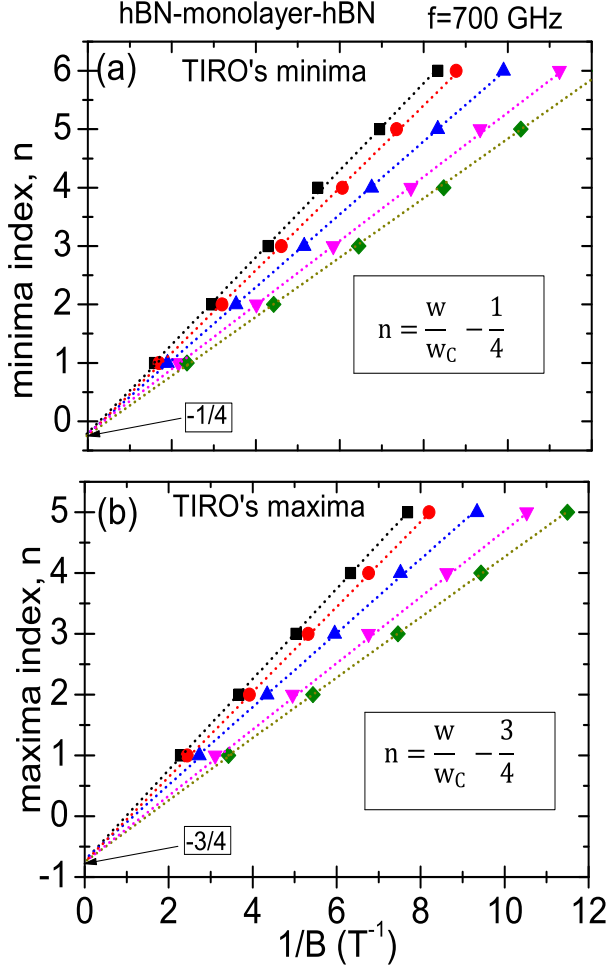


FIG. 3: TIRO's extrema vs the inverse of the magnetic field. In the top panel we exhibit the minima index of Fig. 2 vs $1/B$. In the bottom panel we represent similar to the top panel for the maxima index. As in MIRO, minima are $1/4$ cycle shifted and maxima $3/4$. The dotted straight lines correspond to the minima and maxima fits. For the minima they converge at $-1/4$ and for the maxima at $-3/4$. This is expected from the theoretical model where the straight line equations are given by $n = \frac{w}{w_c} - \frac{1}{4}$ for the minima position and by $n = \frac{w}{w_c} - \frac{3}{4}$ for the maxima (see insets in both panels).

instance at the K point, is given by:

$$H_K = \begin{pmatrix} \Delta & v_F \pi_- \\ v_F \pi_+ & -\Delta \end{pmatrix} \quad (1)$$

$v_F \simeq 1 \times 10^6$ m/s is the Fermi velocity, $\pi_{\pm} = \pi_x \pm i\pi_y$, $\pi_x = P_x$ and $\pi_y = P_y + eBx$, where we have used the Landau gauge, $\vec{A} = (0, Bx, 0)$. Δ is a massive term that represents the potential asymmetry between the two sites. The hamiltonian for the K' valley is the same as for the K but exchanging π_- by π_+ . The corresponding eigenenergies and eigenfunctions can be readily calculated^{55,56},

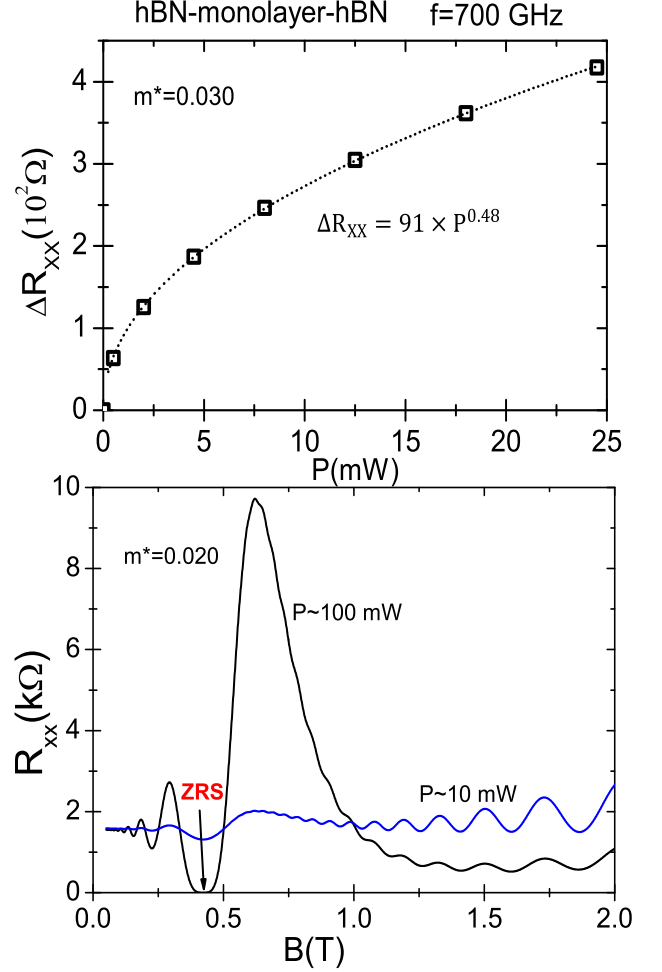


FIG. 4: Radiation power dependence of TIRO for a radiation frequency of 700 GHz. Upper panel: Irradiated magnetoresistance amplitude of minimum 1 of $m^* = 0.030m_e$ curve in Fig. 2 vs radiation power. As in standard MIRO in semiconductor platforms, the calculated curve follows a sublinear relation (square root). In this case, $\Delta R_{xx} = 0.91 \times P^{0.48}$. Lower panel: irradiated R_{xx} vs B for $m^* = 0.020m_e$ case and two different powers, $P = 10$ mW and $P = 100$ mW. For the latter case we show that for a much higher radiation power it is possible to reach a ZRS regime at $B \sim 0.4$ T. $T = 1$ K.

for the K valley:

$$E_{n,K} = \pm \sqrt{(\hbar w_B)^2 |n| + \Delta^2}; (n = \pm 1, \pm 2, \dots) \quad (2)$$

$$E_{0,K} = -\Delta \quad (3)$$

for the energies and

$$\Phi_{n,K} \propto \begin{pmatrix} \phi_{|n|-1} \left(x + \frac{\hbar k_y}{eB} \right) \\ \phi_{|n|} \left(x + \frac{\hbar k_y}{eB} \right) \end{pmatrix} \quad (4)$$

for the eigenstates, where ϕ_n is the standard Landau level

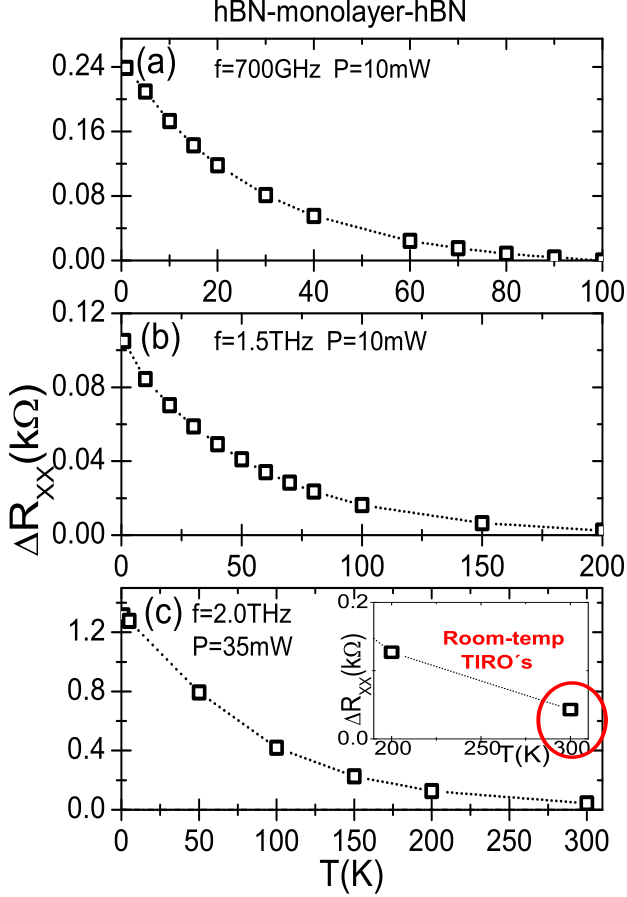


FIG. 5: Temperature dependence of the irradiated magnetoresistance for frequencies of 700GHz in the upper panel, 1.5 THz in the middle and 2 THz in the lower. Radiation-induced oscillations persist at temperatures as high as 100K in the upper panel and 200K in the middle panel. In the lower one we present the striking result of observation of small TIRO at room T. In the inset of the lower panel we exhibit a zoom-in of $T > 200K$ region showing in detail the existence of TIRO at room T

wave function (Landau state) and $w_B = v_F\sqrt{2}/l_B$, l_B being the magnetic length.

For the K' valley:

$$E_{n,K'} = \pm \sqrt{(\hbar w_B)^2 |n| + \Delta^2}; (n = \pm 1, \pm 2, \dots) \quad (5)$$

$$E_{0,K'} = \Delta$$

(6)

and

$$\Phi_{n,K'} \propto \begin{pmatrix} \phi_{|n|} \left(x + \frac{\hbar k_y}{eB} \right) \\ \phi_{|n|-1} \left(x + \frac{\hbar k_y}{eB} \right) \end{pmatrix} \quad (7)$$

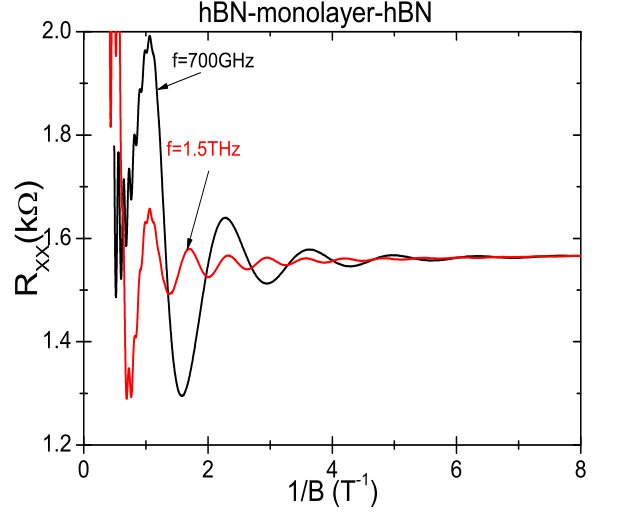


FIG. 6: Frequency dependence of irradiated magnetoresistance vs the inverse of the magnetic field. The exhibited frequencies are 700GHz and 1.5THz. We observe that as frequency increases the magnetoresistance oscillations amplitude get smaller. $T = 1$ K.

An important point of the gapped monolayer graphene eigenstates is that at low lying energies in the conduction band, the amplitude of the wave function at the A site is predominant^{55–57}, i.e., $|\phi_{|n|-1}| \gg |\phi_{|n|}|$ for the K valley and $|\phi_{|n|}| \gg |\phi_{|n|-1}|$ for the K' valley. Accordingly, close to the conduction band bottom we can approximately express the eigenstates at the K valley as,

$$\Phi_{n,K} \propto \begin{pmatrix} \phi_{|n|-1} \left(x + \frac{\hbar k_y}{eB} \right) \\ \sim 0 \end{pmatrix} \quad (8)$$

and a similar expression with $\phi_{|n|} \left(x + \frac{\hbar k_y}{eB} \right)$ for $\Phi_{n,K'}$. Thus, close to the conduction band bottom in the gapped monolayer graphene the Dirac fermions are A-sublattice-polarised. On the other hand, for eigenstates lying close to top of the valence band the amplitude of the wave function is predominant at the B sublattice and then, they are B-sublattice polarised. The complete sublattice pseudospin polarisation is only achieved right at the bottom (top) of the conduction (valence) band. In the framework of the above approximation, we can go further and expand the hamiltonian near the conduction band bottom and obtain an effective expression for the Hamiltonians at the K and K' valleys⁵⁵,

$$H_K \simeq \frac{v^2}{2\Delta} \pi_- \pi_+ = \frac{\pi^2}{2m^*} - \frac{\hbar w_c}{2} \quad (9)$$

$$H_{K'} \simeq \frac{v^2}{2\Delta} \pi_+ \pi_- = \frac{\pi^2}{2m^*} + \frac{\hbar w_c}{2} \quad (10)$$

The cyclotron frequency $w_c = eB/m^*$, m^* being the ef-

fective mass of the corresponding *massive Dirac fermion*,

$$m^* = \frac{\Delta}{v_F^2} \quad (11)$$

Thus, m^* turns out to be gap dependent and can be tuned, for instance by an external bias or by changing the substrate. According to the above, for the eigenstates close to bottom of the conduction band and using the effective expressions of the Hamiltonians $H_{K/K'}$ we can write the next equation for a stationary scenario,

$$\left[\frac{P_x^2}{2m^*} + \frac{(P_y^2 + eBx)}{2m^*} \mp \frac{1}{2}\hbar\omega_c \right] \Phi_{n,K/K'} = E_{n,K/K'} \Phi_{n,K/K'} \quad (12)$$

which is the Schrödinger equation in the presence of a static B . To obtain this equation we have taken into account that $\pi^2 = \pi_x^2 + \pi_y^2$ and the expressions for π_x and π_y . The $'-'$ sign would correspond to K and $'+'$ to K' .

To address magnetotransport in gapped graphene in the presence of radiation and B , we apply the *radiation-driven electron orbits model* that was developed^{24,37} to deal with MIRO and ZRS in high mobility 2D Schrödinger electrons system (GaAs/AlGaAs heterostructures). Its application to massive Dirac fermions starts off from the above stationary equation. The corresponding stationary Hamiltonian can be turned into time-dependent including radiation (time-dependent) and thus,

$$H(t) = \frac{P_x^2}{2m^*} + \frac{1}{2}m^*\omega_c^2(x - X)^2 - eE_{dc}X + \frac{1}{2}m^*\frac{E_{dc}^2}{B^2} - eE_0x \cos \omega t \quad (13)$$

E_{dc} is the driving DC electric field responsible for the current, X is the center of the Landau state orbit: $X = -\frac{\hbar k_y}{eB} + \frac{eE_{dc}}{m^*\omega_c^2}$ and E_0 the intensity of the radiation field. $H(t)$ can be exactly solved allowing a solution for the massive Dirac fermion wave function (for the K valley):

$$\Phi_{n,K} \propto \left(\phi_{|n-1|} \left(x + \frac{\hbar k_y}{eB} - x_{cl}(t), t \right) \right) \quad (14)$$

The time-dependent guiding center shift $x_{cl}(t)$ is given by:

$$x_{cl}(t) = \frac{e^{-\gamma t/2} e E_0}{m^* \sqrt{(\omega_c^2 - \omega^2)^2 + \gamma^4}} \sin \omega t = A(t) \sin \omega t \quad (15)$$

Then, the wave function of $H(t)$ under radiation is the same as in the dark where the center is displaced by $x_{cl}(t)$. Therefore, according to this model the radiation-driven Landau states, occupied by sublattice-polarised massive Dirac fermions, spatially and harmonically oscillate through the guiding center with the radiation frequency performing classical trajectories. This behaviour

resembles the collective motion of electric charge. i.e., a plasmon-like mode, but in this case driven by radiation.

In this swinging motion electrons interact with the lattice ions resulting in a damping process and giving rise to acoustic phonons. They can interact as well with different sources of disorder: defects such as graphene wrinkles and corrugations and with the sample edges yielding the damping of the plasmon-like mode. The damping is phenomenologically introduced through the γ -dependent damping term in the previous $x_{cl}(t)$ equation. Accordingly, the damping of the Landau states-plasmon-like motion comes mainly from two sources. One is temperature independent where we include disorder coming from graphene wrinkles and corrugations and the sample edges. The second is temperature dependent and comes from the interactions of electrons with acoustic phonon modes (lattice ions). Thus, we calculate γ according to the phenomenological expression $\gamma = a + b(T)$, a being an average frequency term representing the driven-Landau states oscillations and accordingly $a \sim 10^{12} \text{ s}^{-1}$, i.e., the parameter a is of the order of the oscillations frequency. $b(T)$ is the electron scattering rate with acoustic phonons that depends linearly with T ⁵⁸⁻⁶⁰ according to $b(T) = 1/\tau_{ac} \simeq (10^{11} - 10^{12}) \times T \text{ s}^{-1}$ for monolayer graphene.

To study the magnetotransport in these systems and calculate R_{xx} we consider the long range Coulomb disorder (charged impurities) as the main source of scattering in graphene⁵⁸. In this scenario an essential result of the model is that, under radiation, the scattering process of electrons with charged impurities turns out to be dramatically modified^{24,25,61-63}. Thus, the key variable is the change of the guiding center coordinate (ΔX) for the Landau states involved in the scattering process⁶⁴. Under radiation ΔX turns into a harmonic function, increasing and decreasing with the radiation frequency. When ΔX increases, we obtain MIRO's peaks in irradiated R_{xx} , and when it lowers we obtain MIRO's valleys. The final expression for the irradiated ΔX is given by^{37,65}:

$$\Delta X = \Delta X(0) - A \sin \left(2\pi \frac{\omega}{\omega_c} \right) \quad (16)$$

where $\Delta X(0)$ is the distance between the guiding centers of the final and initial Landau states in the dark.

We use a semiclassical Boltzmann theory to calculate the longitudinal conductivity σ_{xx} ^{58,64,66-68}:

$$\sigma_{xx} = 2e^2 \int_0^\infty dE \rho_i(E) (\Delta X)^2 W_I \left(-\frac{df(E)}{dE} \right) \quad (17)$$

being E the energy, $\rho_i(E)$ the density of initial Landau states and $f(E)$ the Fermi distribution function. W_I is the scattering rate of electrons with charged impurities that according to the Fermi's golden rule^{58,67,69}: $W_I = \frac{2\pi}{\hbar} |\langle \phi_f | V_s | \phi_i \rangle|^2 \delta(E_i - E_f)$, where ϕ_i and ϕ_f are the wave functions corresponding to the initial and final Landau states respectively and V_s is the scattering

potential for charged impurities^{58,68}. E_i and E_f are the initial and final Landau states energies. To obtain R_{xx} we use the standard tensorial relation $R_{xx} = \frac{\sigma_{xx}}{\sigma_{xx} + \sigma_{xy}}$, where $\sigma_{xy} \simeq \frac{n_i e}{B}$, n_i being the electrons density and e the electron charge.

III. RESULTS

In Fig. 1 we exhibit irradiated magnetoresistance vs B for a bilayer heterostructure of hBN and monolayer graphene. The three curves on the graph correspond to frequencies of 700GHz, 1THz and 2THz and $T = 1.0K$. The inset displays a schematic diagram of the experimental setup main features and the band diagram of gapped monolayer graphene. The electron effective mass used in the simulations is $m^* = 0.0045m_e$ ⁴⁹ where m_e is the bare electron mass. Due to the low effective mass this system turns out to be sensitive to a much higher radiation frequency than the usual MIRO. Thus, we obtain distinctive magnetoresistance oscillations at frequencies clearly in the terahertz region and even close to the far infrared. As in MIRO, we obtain in TIRO that the oscillations become increasingly smaller as the frequency gets bigger keeping constant the radiation power. Remarkably enough, the oscillations are mostly revealed at very low magnetic fields, $B \leq 0.4$ T.

In Fig. 2 we exhibit irradiated magnetoresistance vs B for a gated hBN encapsulated monolayer graphene. The radiation frequency is 700GHz and $T = 1.0K$. The inset shows the basic experimental set up: irradiated hBN sandwiched monolayer graphene under B . We also exhibit two schematic gapped graphene band diagrams at the lower and the upper part of the figure. The lower one corresponds to the lowest external applied bias. This means less injected electrons and a lower Fermi energy. The green curve would represents this scenario. The upper band diagram corresponds to the highest applied bias giving rise to more injected electrons and a higher Fermi energy. This would correspond to the black curve. The hBN layers induce a bandgap in the monolayer graphene that can be tuned by means of the vertical external bias between the two outer hBN layers⁷⁰. Thus, we can select the Dirac fermions effective mass. Based on a previous work⁷⁰, the external bias we have used in the simulations ranges from 0.40 V/Å to 1 V/Å that correspond to band gaps from 230 meV to 340 meV. Eventually, we have used five different effective masses, $m^* = \Delta/v_F^2$, ranging from $0.020m_e$ to $0.030m_e$. Thus, we present in Fig. 2 five curves each one corresponding to a different m^* . Likewise the case in Fig. 1, the current systems turns out to be sensitive to THz radiation and the oscillations turn up at low B ($B \leq 1$ T). As expected, when increasing the external bias (effective mass) the oscillations shift to higher B and the number of oscillations increases too.

These new oscillations or TIRO fulfill the basic characteristics of previous MIRO in semiconductor heterostructures. A remarkable example is exhibited in Fig. 3 where

we present the TIRO minima (upper panel) and maxima (lower panel) index vs the inverse of B . The numerical values for both panels correspond to the $m^* = 0.030m_e$ curve of Fig. 2. We represent the fits for minima and maxima and the obtained dependence between the index n and $1/B$ turns out to be an straight line. For the minima the fits converge at an intercept of $-1/4$ and at $-3/4$ for the maxima. Thus, as in MIRO^{37,65}, minima B -positions are $1/4$ phase shifted and maxima are $3/4$ phase shifted. These results are expected from the model. Thus, for the minima position it is obtained that, $n = \frac{w}{w_c} - \frac{1}{4}$ and for the maxima, $n = \frac{w}{w_c} - \frac{3}{4}$. These equations are in the insets. This has been confirmed by recent experimental results⁴⁶.

In Fig. 4 we exhibit the radiation power dependence of TIRO for hBN encapsulated graphene and a frequency of 700 GHz. In the upper panel we present the irradiated magnetoresistance amplitude of minimum 1 of the $m^* = 0.030m_e$ curve in Fig. 2 vs radiation power. As in standard MIRO in semiconductor platforms, the calculated curve follows a sublinear relation, close to a square root function: $\Delta R_{xx} \propto \sqrt{P}$. For our case we have obtained, $\Delta R_{xx} = 91 \times P^{0.48}$ from the fit. In the lower panel we present irradiated R_{xx} vs B for the $m^* = 0.020m_e$ case and two different powers, $P = 10$ mW and $P = 100$ mW. Thus, for the latter case we predict that for a much higher radiation power it would be possible to reach a ZRS regime for irradiated massive Dirac fermions at $B \sim 0.4$ T for a frequency of 700 GHz.

In Fig. 5 we present the temperature dependence of TIRO for hBN encapsulated monolayer graphene. We exhibit three panels of the irradiated R_{xx} amplitude vs T for three different frequencies, 700 GHz (upper panel), 1.5 THz (middle panel) and 2 THz (lower panel). The exhibited amplitudes for the three of them correspond to the minimum 1 of the $0.030m_e$ curve of Fig. 2. As in MIRO, all of them show that for increasing T the TIRO amplitudes get smaller. For the upper panel we obtain visible TIRO up to around 100 K, and for the middle one we reach 200 K. Interestingly enough, for the lower panel we obtain the striking result that for the highest frequency it would be possible to observe TIRO at room temperature (300 K). A zoom-in between 200 K and 300 K shows clear, although small, oscillations at 300 K.

In Fig. 6 we exhibit the frequency dependence of TIRO for hBN encapsulated graphene. We represent two curves of irradiated R_{xx} vs the inverse of B for frequencies of 700 GHz and 1.5 THz. As in Fig. 1 we obtain much smaller TIRO for higher frequencies. Other simulations with bigger frequencies (not shown) have been run confirming this trend.

IV. CONCLUSIONS

Summing up, we have presented a theoretical approach on the rise of radiation-induced magnetoresistance oscillations in graphene systems of massive Dirac fermions.

- ³⁸ J. Inarrea and G. Platero, Appl. Phys. Lett. **93**, 062104 (2008).
- ³⁹ Jesus Iñarrea and Gloria Platero, Phys. Rev. B **51**, 5244 (1995).
- ⁴⁰ Y.M. Beltukov and M.I. Dyakonov Phys. Rev. Lett. **116**, 176801 (2016)
- ⁴¹ M.A. Zudov et al. Phys. Rev. B **89**, 125401, (2014)
- ⁴² Chepelianskii, A. D., Watanabe, N., Nasyedkin, K., Kono, K. and Konstantinov, D. Nat. Comm. **6**, 7210, (2015)
- ⁴³ Karcher, D. F. et al. Phys. Rev. B **93**, 041410 (2016)
- ⁴⁴ K.S. Novoselov et al. Science, **306**, 666, (2004)
- ⁴⁵ R. G. Mani, A. Kriisa, and R. Munasinghe, Scientific Reports **9** 7278 (2019).
- ⁴⁶ E. Mönch, et al. Nano Lett. **20**, 5943, 2020.
- ⁴⁷ B. Hunt, J. D. Sanchez-Yamagishi, A. F. Young, K. Watanabe, T. Taniguchi, P. Moon, M. Koshino, P. Jarillo-Herrero and R. C. Ashoori. Science, **340**, 1427-1430, (2013).
- ⁴⁸ M. Kindermann, Bruno Uchoa, and D. L. Miller, Phys. Rev. B **86**, 115415 (2012).
- ⁴⁹ Gianluca Giovannetti, Petr A. Khomyakov, Geert Brocks, Paul J. Kelly, and Jeroen van den Brink, Phys. Rev. B **76**, 073103 (2007).
- ⁵⁰ Klaus Zollner, Martin Gmitra, and Jaroslav Fabian, Phys. Rev. B **99**, 125151, (2019).
- ⁵¹ O. V. Kibis, K. Dini, I. V. Iorsh and I. A. Shelykh, Phys. Rev. B, **95** 125401 (2017)
- ⁵² Andrii Iurov, Godfrey Gumbs, and Danhong Huang Phys. Rev. B, **99** 205135 (2019)
- ⁵³ V.P. Gusynin, S.G. Sharapov, J.P. Carbotte, Int. J. Mod. Phys. B **21** 4611-4658 (2007)
- ⁵⁴ V.P. Gusynin and S.G. Sharapov, Phys. Rev. B **71** 125124 (2005)
- ⁵⁵ M. Koshino and T. Ando, Phys. Rev. B **81**, 195431, (2010)
- ⁵⁶ Marko M. Grujic, Milan Z. Tadic and Francois M. Peeters, Phys. Rev. B **90**, 205408, (2014)
- ⁵⁷ J.L. Cheng and C. Guo, Phys. Rev. B **97**, 125417, (2018)
- ⁵⁸ S. Das Sarma, Shaffique Adam, E. H. Hwang, and Enrico Rossi Rev. Mod. Phys. **83**, 407 (2011).
- ⁵⁹ E.H. Hwuang and S. Das Sarma, Phys. Rev. B. **77** 115449 (2008).
- ⁶⁰ Alessandro Principi, Matteo Carrega, Mark B. Lundberg, Achim Woessner, Frank H. L. Koppens, Giovanni Vignale, and Marco Polini, Phys. Rev. B. **90** 165408 (2014).
- ⁶¹ J. Inarrea and G. Platero, Appl. Phys. Lett. **89**, 172114, (2006)
- ⁶² E.H. Kerner, Can. J. Phys. **36**, 371 (1958).
- ⁶³ K. Park, Phys. Rev. B **69** 201301(R) (2004).
- ⁶⁴ Noboru Miura, *Physics of Semiconductors in High Magnetic Fields.*, Oxford University Press, (2008).
- ⁶⁵ Jesus Inarrea and Gloria Platero. Journal of Physics:Condens. Matter, **27** 415801 (2015)
- ⁶⁶ Serban Titeica, Annalen der Physik, **414** 129 (1935)
- ⁶⁷ B.K. Ridley. *Quantum Processes in Semiconductors*, 4th ed. Oxford University Press, (1993)
- ⁶⁸ T. Ando, A. Fowler and F. Stern, Rev. Mod. Phys. **54**, (1982)
- ⁶⁹ B.M. Askerov, *Electron Transport Phenomena in Semiconductors.*, World Scientific, (1994).
- ⁷⁰ Ruge Quhe, Jiaxin Zheng, Guangfu Luo, Qihang Liu, Rui Qin, Jing Zhou, Dapeng Yu, Shigeru Nagase, Wai-Ning Mei, Zhengxiang Gao and Jing Lu, NPG Asia Materials **4**, page 6, (2012).